The Gravity Field of the Moon from the Lunar Prospector Mission

A. S. Konopliv, A. B. Binder, L. L. Hood,
A. B. Kucinskas, W. L. Sjogren, J. G. Williams

A. S. Konopliv, A. B. Kucinskas, W. L. Sjogren, J. G. Williams, Jet Propulsion Laboratory,
 Pasadena, CA 91109
A. B.Binder, Lunar Research Institute, Gilroy, CA 95020
L. L. Hood, University of Arizona, Lunar and Planetary Laboratory, Tucson, AZ 85721

Abstract

The Lunar Prospector (LP) spacecraft has provided the first polar low altitude measurement of the lunar gravity field and as a result gives significant improvement in the lunar gravity field model. The gravity solution with the new LP data clearly reveals three new mascons ("mass concentrations") on the near side of the Moon for the large impact basins Mare Humboltianum, Mendel-Ryberg, and Schiller-Zucchius. Although there is no direct measurement of the lunar farside gravity, LP partially resolves four mascons in the large farside basins of Hertzsprung, Coulomb-Sarton, Freundlich-Sharonov, and Mare Moscoviense and clearly shows a central gravity high in these basin centers. Thus mascons have become more apparent for large impact basins that show no visible mare fill and for farside impact basins. The improvement in the gravity field's second degree harmonics has also improved the normalized polar moment of inertia ($C/MR^2 = 0.3932 \pm 0.0002$) by about a factor of five over previous estimates. This indicates a lunar core with a most probable radius of more than 300 km for an iron composition. The gravity model also determines the long-term spacecraft altitude behavior, and, hence, fuel needs of future missions returning to the Moon.

The gravity field of the Moon has been investigated since the early days of space exploration. In April 1966 the Russian Luna 10 was placed in orbit about the Moon and provided the first dynamical proof that the oblateness of the Moon's gravitational potential (1) was far larger than the shape predicted from hydrostatic equilibrium. During that same year in August of 1966, the first U.S. Lunar Orbiter (LO-I) was launched and four more (LO-II, III, IV, and V) were placed in orbit by August of 1967 with various orbital inclinations and eccentricities. Many investigators analyzed the tracking data for detailed structure in the gravity field using a low-degree spherical harmonic expansion of the gravity field (2, 3). Muller and Sjogren (4), using a rather novel technique of differentiating the Doppler residuals, produced a frontside gravity map that displayed sizable positive gravity anomalies within the large circular mare basins which had topographic lows. This discovery was unexpected and opposite of any physical model at that time and started the development of new models of the Moon's interior. The features were called mascons (short for "mass concentrations"). In addition to the Lunar Orbiters, the Apollo 15 and 16 missions in 1971 released two subsatellites with S-band transponders that provided substantial low altitude tracking data. From these data and also from tracking of the Apollo CSMs, many additional line-of-sight analyses of the data were performed (5) as well as some surface mass distribution models (6, 7).

Further spherical harmonic analyses of the lunar gravity were continued into the late 1970s (8, 9), but to, at most, degree and order 16. The resolution of the gravity solutions was limited due to the extensive computational time required. However, with the availability of improved computer power in the 1990s, the resolution was extended to degree and order 60 (~3600 parameters) using all the available historical data from Lunar Orbiters I-V, and from the Apollo 15 and 16 subsatellites (10). More recently, Clementine tracking data was included with the same historic Lunar Orbiter and Apollo data (11). The Clementine data, from an elliptical orbit with a higher periapse altitude of 400 km, provided improvement in the low degree (n=2,3) and sectoral terms (to degree 20) of the gravity field. The Clementine laser altimetry data, however, provided the

global shape of the Moon for the first time allowing for dramatic improvement in physical modeling of the Moon *(12)*.

Lunar Prospector (LP) is in the first circular polar orbit with a low altitude *(13)* and greatly improves the resolution for the nearside high latitude areas (outside ±30°of the equator). In addition, there is also some improvement for the nearside equatorial region. The gravity information comes from tracking the spacecraft with the JPL's Deep Space Network (DSN) in California, Spain, and Australia, and thus, measuring the line-of-sight velocity from the Doppler shift to an accuracy of 0.2 mm/s for 10-second intervals (or one part in 10^7). Relative to the near side, lunar farside gravity is poorly determined because the spacecraft is not in view from the Earth when over the lunar far side. However, some information is obtained by observing changes in the LP orbit due to the accumulated acceleration of the farside gravity as the spacecraft comes out of occultation *(14)*.

The first three months of data from continuous tracking of LP have been combined with the historical data (LO, Apollo, and Clementine) to produce a 75th degree and order spherical harmonic gravity model *(15)*. In solving for the gravity field *(16,17)*, the last few degrees of the solution are corrupted by unmodeled gravity beyond degree 75 and the lack of farside tracking contributes significantly to noise in the gravity solution. For this reason, the gravity field, which is globally displayed in Fig. 1, contains the acceleration at the lunar surface truncated at degree 70 for the near side and degree 50 for the far side and provides a much cleaner map at the surface compared to the Lun60d model *(10)*. Our model corresponds to a half-wavelength resolution of 75 km, although the nearside data supports a higher resolution and the farside resolution is about 200 km. Evident on the near side are the five principal mascons from the mare filled impact basins Imbrium (20°W, 37°N), Serenitatis (18°E, 26°N), Crisium (58°E, 17°N), Humorum (39°W, 24°S), and Nectaris (33°E, 16°S) that were known from previous missions. Although the far side is somewhat lumpy (an artifact of not having direct farside data), the major basins are visible such as Hertzsprung (130°W, 0°N), Korolev (160°W, 5°S), and Mendeleev (142°E, 5°S). The farside

basins of Hertsprung and Mendeleev were first noticed by Ananda (7) and improved farside resolution for these and others followed (10, 11).

The gravity field of the Moon strongly influences the altitude of a spacecraft in low circular orbit. The most dramatic example is the Apollo 16 subsatellite (i=10°). After being deployed in a near circular orbit from the CSM, the eccentricity increased quickly and the spacecraft impacted the lunar surface 35 days after the release strictly due to the force of the gravity field (the subsatellites had no propulsive systems to raise their altitude). The Apollo 15 subsatellite (i=30°), however, lasted for several years. This long term behavior of the spacecraft is dependent on the inclination (i) of the orbit plane to the lunar equator. Since LP was the first polar (i=90°) circular orbit, there were large uncertainties associated with both the long-term trends in the orbit and, thus, the fuel required to maintain a near circular orbit.

For LP's initial circular orbit, Fig. 2 displays the wide range of predicted periapse altitude trends for various gravity models as well as the actual long term trend we have observed, which is equivalent to a prediction with the model of this paper. The more recent Clementine or GLGM2 model (11) diverges from the actual trend about 15 days into the prediction and this deviation is due to errors in the harmonics as low as degree 10 but is consistent with accuracy of the global field prior to LP. However, the observed long term trend was very close to Lun60d (10) used for planning of the LP mission. The effect of the mascons on the orbit is very clearly evident in the monthly variations in the orbit with 20 km amplitudes. For LP and Apollo 16, the five principal nearside mascons are the major contributor to the long term altitude decline. With the determination of the orbit behavior, LP has also determined the fuel requirements (18) for any future polar lunar mapping missions.

The strength or roughness of the lunar gravity field is given by the amplitude of the gravity coefficients versus degree n (Fig.3A). For the Earth and Venus, the spectrum has empirically been shown to follow a power law $\sim 1/n^2$ (or Kaula rule, 16) with the constant scaled for each planet to allow the same level of stress. For the Earth scaled to the Moon, the leading constant for the power law is 3.5×10^{-4} and is greater than the measured spectrum for the Moon indicating it is closer to

equilibrium than the Earth *(19,9)*. Our best power law fit to the spectrum is $1.2 \times 10^{-4}/n^{1.8}$, and is also close in power to the Lun60d model *(10)*. The spectrum is reliable to about degree 20, but beyond that, the power in the spectrum has large uncertainties due to the lack of farside data. Although it is clear that the true spectrum will have more power for the medium to short wavelengths than the GLGM2 gravity model *(11)*. If a constraint is not applied to the gravity solution *(20)*, then the spectrum quickly deviates from the power law at degree 12 indicating that there are substantial errors in the coefficients beyond that degree and the need for direct farside gravity data.

With a gravity data set that is closer to global, the coherence with topography *(21)* has also increased (Fig. 3B) for the mid-wavelength frequencies ($n = 20$ to 50). If we had farside gravity data, it would be expected to substantially increase the correlations and thus the admittance (Fig. 3C) indicating a greater globally averaged percent of Airy isostatic compensation of the surface topography for those degrees. Even so, global compensation is more apparent than previous models *(12)* for this frequency range. The anticorrelation of gravity and topography, due in part to the five principal nearside mascons, is evident in degrees 10 to 20 and the tailing of the correlation at high degree is probably due in part to the limited topographic sampling for those frequencies (60 km spacing between altimetry tracks) and reduction in farside gravity information.

A striking result from the LO and Apollo lunar gravity data was the lunar mascons *(4)*. Indeed, the observation of large, positive gravity anomalies centered in many of the lunar basins indicate large buried mass anomalies which are uncompensated. A possibly related discovery consists of the negative gravity anomalies observed over the ejecta blankets surrounding mascon basins *(22)* suggesting a ring of mass deficit around the mascons. The mascons known at that time were all on the near side of the Moon and were filled with maria several kilometers thick. With the new LP data, seven new large mascons have been identified where there is a clear maximum in the gravity at the center of each basin. Of the three new mascons on the near side of the Moon (see Fig. 4), Mare Humboltianum (80°E, 57°N) has lava fill, Mendel-Rydberg (95°W, 50° S) has some mare fill and possibly more covered by Mare Orientale ejecta *(23)*, and Schiller-Zucchius (45°W,

5

55°S) shows no evidence of mare fill. Of the four new mascons on the far side of the Moon, only Mare Moscoviense clearly has mare fill, the others being Hertzsprung (130°W, 2°N), Coulomb-Sarton (120°W, 51°N), and Freundlich-Sharonov (175°E, 18°N). The amplitudes of the farside mascons have large uncertainties. Currently, the differences between the negative basin ring and the maximum in the basin center (100 to 150 mgals) are about one-half to one-third of the ranges for the non-mare filled nearside mascon basins, and this indicates that the farside amplitudes may be underestimated by a factor of three.

Several processes have been proposed to explain the formation and support mechanism of lunar mascons (see reviews in *19, 24*). One popular scenario hypothesizes that giant impacts only created favorable locations (namely, the circular basins) where molten basalt from the interior could pond *(25)*. Indeed, several authors argue that following a giant impact the extensive excavation of lunar material resulted in crater relaxation, a strong thermal anomaly, and high levels of stress *(26)*. According to this model, the heating and weakening of the crust in this area allowed an upwelling of dense mantle rock resulting in excess mass near the center of the basin *(27-29)*. This mantle rebound resulted in Moho uplift and the formation of a dense mantle "plug". At this time, the basins were in near isostatic equilibrium but a deep depression remained. Subsequently, the remaining depression in the basin was filled with flood basalts. This resulted in the mascons as uncompensated buried loads (or, as referred to by some authors, a "superisostatic" situation) in the mascon basins. Wise and Yates *(27)* further propose that the weight of the highlands surrounding the mascon basins forced lava laterally over the mare floor once isostatic equilibrium had been reached following the rise of the high density material; this model correctly predicts the negative gravity anomaly ring observed around the mascons *(22)*.

For the previously described essentially "passive" mascon formation scenario the buried load responsible for the mascon anomalies is the result of the combination of the dense mantle plug and the basin fill *(30)*. However, in the context of this model, the question of the respective contribution of mantle plug and subsequent mare fill to the observed positive mascon gravity anomaly is a matter of debate. Indeed, some authors *(27)* believe that the mare fill is of relatively

low density and that most of the positive mascon anomaly is due to the high density mantle plug and some (31) believe that what is seen is a combination of the two. On the other hand, other researchers (28) used Apollo gravity data to argue that the mass anomalies responsible for the five principal mascons (in particular, Mare Serenitatis) are thin and near the surface: in their view, the dominant contribution to the mascon gravity anomalies comes from a high density mare fill (relative to the crust) rather than from the deep uplifted mantle plug. Their arguement stems from the strong shoulders seen in the line-of-sight data. Likewise, the gravity model presented here does show a plateau for the principal mascons (see Fig. 5) not seen in the GLGM2 model (11). The LP extended mission with 10-40 km altitude data will provide further data to separate out the contributions of maria and mantle plug.

Also debated is the question of mantle rebound. Dvorak and Phillips (32) argued against a slow isostatic mantle response with upwelling of the dense lunar mantle. Following a suggestion by Taylor (33), Neumann et al. (34) used Clementine topography and gravity data to argue in favor of a dynamic or "active" rather than long-term isostatic adjustment mechanism of mantle upwelling. In their view, the mascon anomalies are essentially due to a combination of rapid mantle rebound, immediately following and a direct cause of the basin-forming impact, and an additional mass excess component from the mare basalt filling which was emplaced at a later date.

Arkani-Hamed (24, 35) also proposes an "active" mascon formation model, relating mascon formation directly to the effect of giant impacts. In this hypothesis, partial melting occurs beneath the surrounding highlands as a consequence of a thermal blanketing effect by the ejecta; molten basalt is then laterally transported from beneath the highlands (resulting in the observed negative gravity anomaly) into the basins (resulting in the positive mascon gravity anomaly).

In addition to the question of how mass was transported to create the mascon anomalies, one must address the problem of how the mascons were maintained since they were emplaced, approximately 3.6 Ga ago (36). For several authors, support of the mascons for the past 3.6 Ga is accomplished through flexure, that is via bending stresses of an elastic layer on the Moon (37). This model could also explain the negative ring around the mascons. Arkani-Hamed (24, 35)

proposes a viscous decay model for support of the mascons, emphasizing the role of viscous deformation of the lunar interior. He argues that the elastic layer of the moon was not thick enough to achieve mascon support at the time of their formation. Elastic support was achieved at a later date (estimated at around 3 Ga ago) when the upper parts of the moon became strong enough.

Several authors have computed lunar crustal thickness maps using Clementine topography and gravity data. These maps were obtained by performing inversions via downward continuing either Bouguer anomalies *(12, 34, 38)* or gravity anomalies *(39)* to yield regional depths to the Moho. Implicit in the calculations is the assumption of Airy isostasy and, for some models, a fixed background Airy crustal thickness (estimated from seismically derived Moho depths at Apollo landing sites). As noted by von Frese et al. *(39)*, one must be careful when interpreting the results of these studies as they are nonunique and sensitive to data errors, model assumptions, and the filtering techniques used for the downward continuation. Using a forward modeling approach, we have produced an Airy crustal thickness map for the moon without making the a-priori assumption of a fixed thickness for the lunar background (or reference) crustal thickness. This allows to test the physical validity of the Airy model for a given region in addition to showing global trends in regional Airy crustal thickness variations.

Fig. 1 shows a map of regional Airy lateral crustal thickness variations obtained using spatial domain Geoid-Topography Ratio (GTR) techniques implemented for Venus *(40)*, with a data window sliding over the lunar surface. For each fixed position of the sliding window, mean values of the spherical harmonic derived geoid anomaly (N) and topography variation (h) are compared, in the least squares sense and in the spatial domain, to theoretical Airy correlations of N and h. This results in a best-fit value of the reference crustal thickness H for the considered region. This value is then added to the mean h and corresponding value of the Airy root (b) to produce a total mean crustal thickness TT for the considered position of the data window (i.e., $TT(h) = h + b(h) + H$). Data used to produce the map is the Clementine lunar topography *(21)* and the gravity solution of this paper produced using Lunar Prospector data. Anomalies are measured with respect to a lunar reference radius of 1738 km and the spherical harmonic data is unfiltered.

Airy compensation seems a viable model for the highlands, with a mean Airy reference crustal thickness of ~70 km. The lowland mascon basins, however, show a negative compensation depth, suggesting that 1-layer Airy isostasy is not valid in these areas. However, note that this map was produced without filtering out the mascon anomalies, so that what we are seeing here is the result of an excess buried mass over a topography low. An interesting feature revealed by this map is the large positive Airy crustal thickness in the large masconless basin of Aitken (near the south pole on the far side), and Procellarum . The Airy thickness is especially large in Procellarum, a possible indication of Pratt isostasy (i.e., lateral variations in crustal density) there.

Since LP is a simple spin-stabilized spacecraft, it is ideal for long wavelength gravity studies because of limited nonconservative forces acting on the spacecraft. The resulting unnormalized second degree values of interest are $J_2 = (203.428 \pm 0.09) \times 10^{-6}$ and $C_{22} = (22.395 \pm 0.015) \times 10^{-6}$ where errors are five times the formal statistic. By combining the LP lunar GM (4902.8003 ± 0.0012) with either the GM(Earth+Moon) from the LLR solution of this paper or the Earth's GM from artificial satellite ranging one gets an Earth-Moon mass ratio of 81.300566+/- 0.000020 (41).

The normalized polar moment of inertia (C/MR^2) or homogeneity constant for the Moon is a measure of the radial density distribution where a value of 0.4 indicates a homogeneous Moon and a value less than 0.4 indicates increasing density with depth (for example the Earth with a sizable core has $C/MR^2 = 0.33$). The solution for the three principal moments of inertia A<B<C depends on four relations given by the lunar libration parameters $\gamma=(B-A)/C$ and $\beta=(C-A)/B$, determined from the Lunar Laser Ranging (or LLR, 42), and the second order gravity harmonics $J_2 = [C - (A+B)/2]/MR^2$ and $C_{22} = (B-A)/4MR^2$. The values for the polar moment have varied significantly mostly due to variations in the solutions for the second degree gravity harmonics (43). The strictly LLR solution is $C/MR^2 = 0.394 \pm 0.002$ (42) and the combination with earlier spacecraft results gives 0.393 ± 0.001 (43). A major contribution to published LLR libration parameter uncertainties (42) is from the C_{31} and C_{33} harmonics. An LLR solution using 28 yr of data, while adopting the LP values of J_2, C_{31}, and C_{33}, gives $\beta = (631.486 \pm 0.09) \times 10^{-6}$ and $\gamma =$

$(227.871 \pm 0.03) \times 10^{-6}$. The β and γ uncertainty is mainly due to the size of a possible core. Combining J_2, C_{22}, β, and γ gives the polar $C/MR^2 = 0.3932 \pm 0.0002$ (an uncertainty of five times the formal error) and the average moment $I/MR^2 = 0.3931 \pm 0.0002$. The uncertainties of J_2 and C_{22} dominate the moment error, although, from the improvement of the second degree harmonics, the resulting uncertainty in C/MR^2 is reduced by about a factor of five over previous estimates. J_2 and C_{22} are consistent with β and γ within the stated uncertainty, which is a welcome improvement over sizable discrepancies noted in many historical values (44).

The lunar polar moment, when combined with compositional, thermal, and density models of the lunar crust and mantle, can allow some useful inferences to be drawn about the mass and size of a possible metallic core (45, 46). For example, Hood and Jones (45) adopted an upper bound on C/MR^2 of 0.3928 (47) and found that calculated mantle density increases (for a variety of possible bulk compositions and temperature profiles) were insufficient to match this upper bound even when the most favorable combinations of allowed crustal thickness and density were assumed. It was therefore concluded that a small Fe-rich core was probably needed with a mass in the range of 1 to 5% of the lunar mass. A consideration of independent geophysical constraints on the core size, mainly derived from Apollo magnetic sounding data (48), refined this estimate further to no more than 4% of the lunar mass. The present determination of C/MR^2 yields an upper bound of 0.3934, only slightly larger than that adopted by Hood and Jones. Consequently, their conclusion that the most probable core mass lies between 1 and 4% of the lunar mass remains unchanged. For an assumed Fe composition, the core radius would lie between about 300 and 450 km.

In a study of the internal structure of a Moon which was initially totally molten and petrologically differentiated, Binder (49) found that the Moon probably has an Fe or Fe-rich core between 200 and 400 km in radius. In his study, Binder evaluated the uncertainties in the core radius due to uncertainties in the crustal composition and thickness, upper-mantle composition and thickness, lower mantle composition, thermal profile, core composition (molten Fe or FeS), coefficients of thermal expansion and bulk modulus of lunar minerals and moment-of-inertia

factor, he assumed that the latter was probably between 0.390 and 0.393 and certainly between 0.389 and 0.394. In suggesting an upper limit of 400 km for the core radius, Binder adopted independent constraints based mainly on magnetic data; however, later assessments increased this upper limit to 450 km *(48)*. Additional evidence implies an upper limit of 330 km for an Fe core and 370 km for FeS that is deduced from the influence of lunar rotational dissipation on the spin axis direction *(50)*.

Using the data and figures of Binder *(49)* and our value of the moment-of-inertia factor (I/MR^2) of 0.3931 ± 0.0002, we find that the radius of an Fe core is 320+50/-100 km and its mass is 1.4+0.8/-0.9% of the Moon's mass. The corresponding radius and mass of a FeS core are 510+80/-180 km and 3.5+1.9/-2.6%, respectively. If the maximum radius of the core is 450 km as derived from the seismic and magnetic data, then the core is probably Fe or Fe-rich, though an FeS core is not excluded by the data and models.

While the inferred existence of a small metallic core with mass exceeding 1% of the lunar mass is indirect and provisional, if verified by future direct measurements, such a core would imply that the Moon is not composed entirely of terrestrial mantle material. The latter bulk composition would result in an Fe-rich core representing only 0.1% to 0.4% of the lunar mass in order to produce observed depletions of lunar siderophile elements *(51)*. In its simplest form, the leading hypothesis for lunar origin, the impact-trigger model predicts a Moon composed primarily of material from the Earth's mantle and the impactor's mantle and, therefore, little or no metallic core *(52)*. However, more recent versions of the model in which the giant impact occurred prior to completion of Earth accretion *(53)* permit the presence of cores in the range inferred here.

(1) E. L. Akim, *D.A.N. SSSR* 170, 799 (1966). Akim's estimate of the gravitational oblateness J_2 (or equatorial bulge)was very close to our present day estimate (within 1%), but his estimate for C_{22} (a lunar bulge in the direction of the Earth-Moon line), however, was 40% too small.

(2) J. Lorell and W. L. Sjogren, *Science* 159, 625 (1968); W. H. Michael Jr. and W. T. Blackshear, *Moon* 3, 388 (1972).

(3) A. S. Liu and P. S. Laing, *Science* 173, 1017 (1971).

(4) P. M. Muller and W. L. Sjogren, *Science* 161, 680 (1968). This then new method of determining the gravity was called "line-of-sight". The Doppler residual, from tracking the spacecraft, measures the velocity in the line-of-sight direction from the tracking station to the spacecraft. The gravity field is found from the Doppler derivative corrected for geometry (mapped to the lunar vertical gravity direction) and spacecraft altitude (downward continued).

(5) W. L. Sjogren, P. Gottlieb, P. M. Muller, W. R. Wollenhaupt, *Apollo 15 Preliminary Science Report* SP-289, 20-1(1972); W. L. Sjogren, W. R. Wollenhaupt, R. N. Wimberly, *Apollo 17 Preliminary Science Report SP-330*, 14-1 (1973); W. L. Sjogren and W. R. Wollenhaupt, *Moon* 8, 25 (1973); W. L. Sjogren, R. N. Wimberly, W. R. Wollenhaupt, *Moon* 9, 115 (1974); R. J. Phillips, J. E. Conel, W. L. Sjogren, *Space Research* XIV, 635 (1974); W. L. Sjogren and J. C. Smith, *Proc. Seventh Lunar Sci. Conf.* 3, 2639 (1976); A. J. Ferrari, D. L. Nelson, W. L. Sjogren, R. J. Phillips, *J. Geophys. Res.* 83, 2863 (1978).

(6) L. Wong et. al., *J. Geophys. Res.* 76, 6220 (1971).

(7) M. P. Ananda, *J. Geophys. Res.* 82, 3049 (1977).

(8) A. J. Ferrari, *J. Geophys. Res.* 82, 3065 (1977).

(9) B. G. Bills and A. J. Ferrari, *J. Geophys. Res.* 85, 1013 (1980).

(10) A. S. Konopliv, W. L. Sjogren, R. N. Wimberly, R. A. Cook, A. Vijayaraghavan, in *Proceedings of the AAS/AIAA Astrodynamics Specialist Conference*, Victoria, BC, 1993,

edited by A. K. Misra, V. J. Modi, R. Holdaway, and P. M. Bainam (Univelt, San Diego, CA, 1993), pp. 1275-1294.

(11) F. G. Lemoine, D. E. Smith, M. T. Zuber, G. A. Neumann, D. D. Rowlands, *J. Geophys. Res.*, 102, 16339 (1997).

(12) M. T. Zuber, D. E. Smith, F. G. Lemoine, G. A. Neumann, *Science* 266, 1839 (1994).

(13) The only polar (i=90°) orbiters were LO-IV, LO-V, and Clementine. All other spacecraft for which we have data have i<30°. The LO polar orbits, however, were also elliptical with the only low altitude data near the lunar equator.

(14) Unlike the line-of-sight technique, our spherical harmonic models are fully dynamic in that they numerically integrate the equations of motion for the spacecraft accounting for all forces such as the gravity field, perturbations of other planets, solar radiation pressure on the spacecraft, and relativistic terms. Since we process the LP data with intervals or arcs of two days, we see the dynamic effect of the far side on 24 orbits at a time. This combined with the dynamic information of the other spacecraft at different inclinations (10° to 30°) and eccentricities gives the total farside gravity we observe.

(15) This gravity solution (LP75G), like the previous solution (LP75D), is available from the Geosciences Data Node of the Planetary Data System (www.pds-geophys.wustl.edu /pds/lunar_prospector) or can be requested from author A. K.

(16) W. M. Kaula in *Theory of Satellite Geodesy*, Blaisdell, Waltham, MA (1966).

(17) The gravity solution is a least-squares determination [see C. L. Lawson and R. J. Hanson in *Solving Least Squares Problems*, Society for Industrial and Applied Mathematics, Philadelphia (1995)] using JPL's ODP software [see T. D. Moyer, *JPL Technical Report 32-1527*, Jet Propulsion Laboratory, California Institute of Technology, Pasadena, CA (1971)].

(18) The fuel usage of the LP mission was based upon the field of Konopliv et al *(10)* which predicted an average of 0.22 m/s/day average fuel usage, but about three times this amount (0.75 m/s/day for a one year mission) was carried because of the large unknowns. If the

actual trend was similar to the Apollo 16 subsatellite, LP would have run out of fuel about halfway through the nominal mission. However, the observed long term trend of 0.25 m/s/day was very close to that assumed with plenty of fuel remaining for an extended mission.

(19) W. M. Kaula, Science 166, 1581 (1969).

(20) To avoid aliasing or large artifacts in the gravity solution, the coefficients are either constrained toward zero with an uncertainty given by a power law ($\sim 1/n^2$), as is done in *(11)* and *(12)*, or a surface constraint is applied that varies spatially depending on the data strength [see A. S. Konopliv, W. B. Banerdt, W. L. Sjogren, *Icarus*, in review (1998)]. For these preliminary models we have used a power constraint but plan to use a spatial constraint in future work.

(21) Greg Neumann, personal communication (1997). This topography model is an update of GLTM2 of D. E. Smith, M. T. Zuber, G. A. Neumann, F. G. Lemoine, *J. Geophys. Res.*, 102, 1591 (1997).

(22) W. L. Sjogren, P. Gottlieb, P. M. Muller, W. Wollenhaupt, *Science* 175, 165 (1972).

(23) P. D. Spudis, R. A. Reisse, J. J. Gillis, *Science* 266, 1848 (1994).

(24) J. Arkani-Hamed, *J. Geophys. Res.* 103, 3709 (1998).

(25) S. K. Runcorn, *Proc. Lunar Sci. Conf.* 5, 3115 (1974); S. C. Solomon, *Proc. Lunar Sci. Conf.* 6, 1021 (1975).

(26) H. J. Melosh and W. B. McKinnon, *Geophys. Res. Let.* 5, 985 (1978); S. C. Solomon, R. P. Comer, J. W. Head, *J. Geophys. Res.* 87, 3975 (1982); S. R. Bratt, S. C. Solomon, J. W. Head, *J. Geophys. Res.* 90, 12415 (1985).

(27) D. U. Wise and M. T. Yates, *J. Geophys. Res.* 75, 261 (1970).

(28) R. J. Phillips, J. E. Conel, E. A. Abbott, W. L. Sjogren, J. B. Morton, *J. Geophys. Res.* 77, 7106 (1972).

(29) S. R. Bratt, S. C. Solomon, J. W. Head, C. H. Thurber, *J. Geophys. Res.* 90, 3049 (1985).

(30) S. C. Solomon and J. W. Head, *J. Geophys. Res.* 84, 1667 (1979).

(31) C. Bowin, B. Simon, W. R. Wollenhaupt, *J. Geophys. Res.* 80, 4947 (1975).

(32) J. Dvorak and R J. Phillips, *Planetary Lunar Conference* 9, 3651 (1978).

(33) S. R. Taylor, *Planetary Science: A Lunar Perspective*, Lunar Planet. Inst., Houston, Texas (1982).

(34) G. A. Neumann, M. T. Zuber, D. E. Smith, F. G. Lemoine, *J. Geophys. Res.* 101, 16841 (1996).

(35) J. Arkani-Hamed, *Proc. Lunar Sci. Conf.* 4, 2673 (1973).

(36) J. W. Head, *Rev. Geophys.* 14, 265 (1976).

(37) H. J. Melosh, *Proc. Lunar Sci. Conf.* 9, 3513 (1978); S. C. Solomon and J. W. Head, *Rev. Geophys.* 18, 107 (1980); R. J. Willemann and D. L. Turcotte, *Proc. Lunar Planet. Sci.* 12B, 837 (1981).

(38) M. A. Wieczorek and R.J. Phillips, *J. Geophys. Res.*, 103, 1715 (1998).

(39) R. R .B. von Frese et al, *J. Geophys. Res.*, 102, 25657 (1997).

(40) A.B. Kucinskas and D.L. Turcotte, *Icarus* 112, 104 (1994); A.B. Kucinskas, D.L. Turcotte, J. Arkani-Hamed, *J. Geophys. Res.*, 101, 4725 (1996), For Fig. 1, we used a density of 2.8 for the crust and 3.3 for the mantle (gm/cm^3).

(41) The LLR Sun/(Earth+Moon) mass ratio is 328900.559 ± 0.002, which gives in TDB units GM(Earth+Moon) = 403503.236 ± 0.002 km3/sec2. The artificial satellite result is GM(Earth)=398600.4356 ± 0.0008 km3/sec2 in TDB units, J. C. Ries, R. J. Eanes, C. K. Shum, and M. M. Watkins, Geophys. Res. Lett. 19, 529 (1992).

(42) J. O. Dickey et. al., *Science* 265, 482 (1994).

(43) J. G. Williams, X X Newhall, J. O. Dickey, *Planet. Space Sci.* 44, 1077 (1996).

(44) B. G. Bills, *J. Geophys. Res.* 100, 26297 (1995).

(45) L. L. Hood and J. H. Jones, *J. Geophys. Res.* 92, E396 (1987).

(46) S. Mueller, G. J. Taylor, R. J. Phillips, *J. Geophys. Res.* 93, 6338 (1988).

(47) A. J. Ferrari, W. S. Sinclair, W. L. Sjogren, J. G. Williams, C. F. Yoder, *J. Geophys. Res.* 85, 3939 (1980).

(48) Hood, L. L. in *Origin of the Moon*, W. K. Hartmann, R. J. Phillips, G. J. Taylor, Eds. (Lunar and Planetary Institute, Houston, 1986), pp. 361-410.

(49) A. B. Binder, *J. Geophys. Res.* 85, 4872 (1980).

(50) C. F. Yoder, *Phil. Trans. Royal Soc. London* A 303, 327 (1981); J. G. Williams , X X Newhall, C. F. Yoder, J. O. Dickey, Lunar Rotational Dissipation in Solid Body and Core, in Abstracts of the Lunar and Planetary Science Conference XXVIII, abstract # 1379, (1997); J. G. Williams, T. P. Krisher, D. H. Boggs, J. T. Ratcliff, J. O. Dickey, Lunar Dissipation: Rotational and Orbital Consequences, in Abstracts of theLunar and Planetary Science Conference XXIX, abstract #1963 (1998).

(51) For example, see H. E. Newsom in *Origin of the Moon*, W. K. Hartmann, R. J. Phillips, G. J. Taylor, Eds. (Lunar and Planetary Institute, Houston, 1986), pp. 203-230.

(52) A. G. W. Cameron, *Icarus* 126, 126 (1997); R. M. Canup and L. W. Esposito, *Icarus* 119, 427 (1996).

(53) A. G. W. Cameron and R. M. Canup, The giant impact occurred during Earth Accretion (abstract), paper presented at 29th Lunar and Planetary Science Conference, Lunar and Planetary Institute, Houston, 1998.

(54) We thank Greg Neumann and Maria Zuber for providing the latest lunar topography solutions from Clementine and Frank Lemoine for his lunar gravity field and spacecraft model information for processing the Clementine tracking data. Helpful discussions with Don Turcotte are greatly appreciated. LLR solutions were done with the help of D. H. Boggs and LP data was processed with the help of E. Carranza and D. N. Yuan. The research described in this paper was carried out by the Jet Propulsion Laboratory, California Institute of Technology, under a contract with the National Aeronautics and Space Administration.

Fig 1. Vertical gravity anomalies from LP75G at the reference surface of the Moon for the (**A**) near side and (**B**) far side using a Lambert equal area projection. The accelerations are in milligals (1 mgal = 10^{-5} m/s^2) and represent the deviation from a uniform sphere with the J_2 contribution to the oblateness also removed. The central mass acceleration is 160,000 mgals and the range of the deviations is about 900 mgals (~0.5% of the total). Crustal thickness (TT) in km with an Airy compensation model for the near side (**C**) and far side (**D**) shows the lunar dichotomy. Procellarum (black region with TT> 220km at 50°W, 20°N) and the center of South-Pole Aitken basin are areas of maximum Airy-depth.

Fig. 2. Predicted periapse altitude behavior for Lunar Prospector for different lunar gravity fields. Periapse altitude occurs every 2 hours when the spacecraft is closest to the Moon when traveling along its elliptical orbit. As the periapse lowers, the furthest point or apoapse of the orbit increases so that the sum or energy is constant. The heavy solid lines show the actual periapse altitude behavior for LP (upper right) and for comparison purposes the actual Apollo 16 subsatellite altitude (lower left). The predicted LP behavior from the GLGM2 model *(11)* is very similar to the Bills-Ferrari model *(9)*, whereas the Liu-Laing *(3)* prediction is similar to the joint LLR / Orbiter based solution *(47)*. Actual behavior is very close to the a priori model used for LP *(10)* (not shown is the burn that was performed 51 days after the initial circular orbit to raise the periapse altitude).
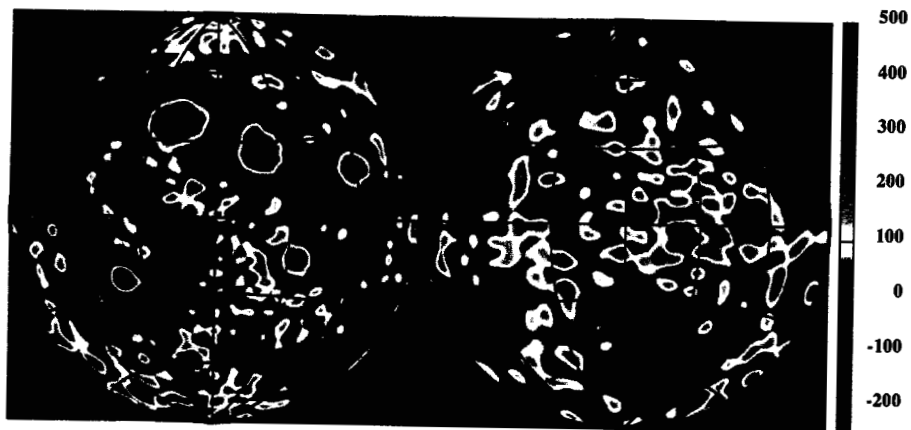
Fig. 3. (**A**) Power spectrum of the lunar gravity field with the heavy solid line the expected power law ($3.5\times10^{-4}/n^2$), the thin solid line from GLGM2 *(11)*, the solid circles from LP75G (this paper), the open circles the errors in the spectrum for LP75G, and the dashed line the spectrum from an unconstrained 50th degree gravity solution. (**B**) The coherence of the topography *(21)* and gravity for LP75G (solid line), GLGM2 (dashed line), and for LP75G with the 5 principal mascons removed (light solid line). (**C**) Admittance between topography and gravity field LP75G (solid

line) and GLGM2 (heavy dashed line). The light dashed lines represent theoretical admittance for Airy isostatic compensation at the depths indicated.

Fig. 4. Displayed are the new mascons for three large impact basins on the near side of the Moon. All are located in high latitude areas where no previous low altitude tracking data existed. The basins are (**A**) Mare Humboltianum, (**B**) Mendel-Rydberg, and (**C**) Schiller-Zucchius. For each, the topography in km is shown first with the gravity (LP75G) mapped to the surface shown second. For comparison, the gravity prior to LP *(11)* is also shown in (**A**). The gravity central peak at the center of the basin is evident and corresponds to the topographic low.

Fig. 5. Topography (top) and surface gravity (bottom) for Mare Serenitatis. The gravity shows a plateau and thus a significant near surface contribution to the mascon. Also apparent is the smaller mascon Mare Vaporum in the lower and left of center part of the figure. Color bar scales are the same as for Fig 4.
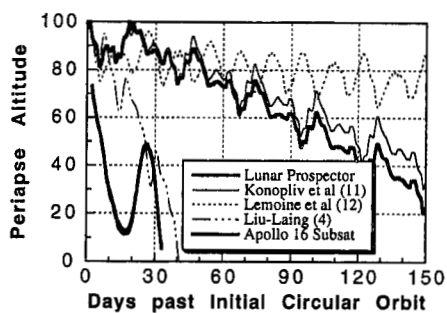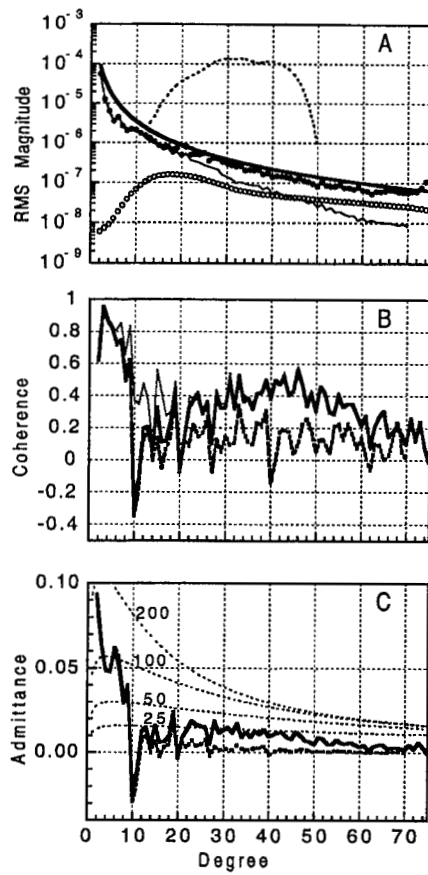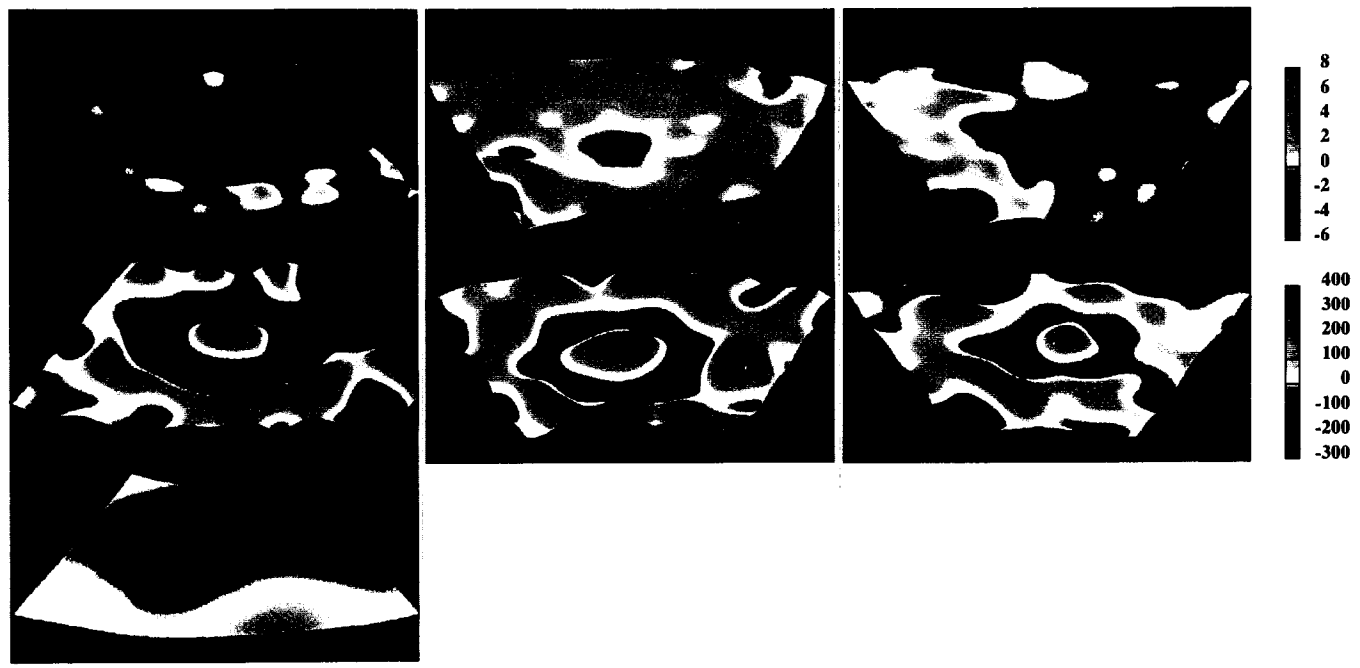
Figure 1

A, B

C, D

Figure 2

Periapse Altitude vs *Days past Initial Circular Orbit*

Legend:
- Lunar Prospector
- Konopliv et al (11)
- Lemoine et al (12)
- Liu-Laing (4)
- Apollo 16 Subsat

Figure 3

Figure 4

(a)   (b.)   (c)

Figure 5